PAPER • OPEN ACCESS

High harmonic interferometry of the Lorentz force in strong mid-infrared laser fields

To cite this article: Emilio Pisanty *et al* 2018 *New J. Phys.* **20** 053036

New Journal of Physics
The open access journal at the forefront of physics

Deutsche Physikalische Gesellschaft DPG
IOP Institute of Physics

Published in partnership with: Deutsche Physikalische Gesellschaft and the Institute of Physics

OPEN ACCESS

RECEIVED
19 December 2017

REVISED
22 March 2018

ACCEPTED FOR PUBLICATION
3 April 2018

PUBLISHED
11 May 2018

PAPER

High harmonic interferometry of the Lorentz force in strong mid-infrared laser fields

Emilio Pisanty[1,2,6,7], **Daniel D Hickstein**[3], **Benjamin R Galloway**[3], **Charles G Durfee**[3,4], **Henry C Kapteyn**[3], **Margaret M Murnane**[3] and **Misha Ivanov**[1,2,5]

[1] Blackett Laboratory, Imperial College London, South Kensington Campus, SW7 2AZ London, United Kingdom
[2] Max Born Institute for Nonlinear Optics and Short Pulse Spectroscopy, Max Born Strasse 2a, D-12489 Berlin, Germany
[3] JILA—Department of Physics, University of Colorado and NIST, Boulder, CO 80309, United States of America
[4] Colorado School of Mines, Department of Physics, Golden, CO 80401, United States of America
[5] Department of Physics, Humboldt University, Newtonstrasse 15, D-12489 Berlin, Germany
[6] Present address: ICFO—The Institute of Photonic Sciences, Barcelona, Spain.
[7] Author to whom any correspondence should be addressed.

E-mail: emilio.pisanty@icfo.eu, danhickstein@gmail.com and m.ivanov@imperial.ac.uk

Keywords: high harmonic generation, strong-field physics, dipole approximation, strong-field approximation, bicircular fields

Abstract

The interaction of intense mid-infrared laser fields with atoms and molecules leads to a range of new opportunities, from the production of bright, coherent radiation in the soft x-ray range, to imaging molecular structures and dynamics with attosecond temporal and sub-angstrom spatial resolution. However, all these effects, which rely on laser-driven recollision of an electron removed by the strong laser field and its parent ion, suffer from the rapidly increasing role of the magnetic field component of the driving pulse: the associated Lorentz force pushes the electrons off course in their excursion and suppresses all recollision-based processes, including high harmonic generation as well as elastic and inelastic scattering. Here we show how the use of two non-collinear beams with opposite circular polarizations produces a forwards ellipticity which can be used to monitor, control, and cancel the effect of the Lorentz force. This arrangement can thus be used to re-enable recollision-based phenomena in regimes beyond the *long*-wavelength breakdown of the dipole approximation, and it can be used to observe this breakdown in high harmonic generation using currently available light sources.

Strong-field phenomena benefit from the use of long-wavelength drivers since, for sufficiently intense fields, the energy of the interaction scales as the square of the driving wavelength, since with a longer period the electron has more time to harvest energy from the field. In particular, long-wavelength drivers allow one to extend the generation of high-order harmonics [1–3] towards the production of short, bright pulses of x-ray radiation, currently reaching into the keV range with thousands of harmonic orders [4], and with driving laser wavelengths as long as 9 μm under consideration [5, 6].

However, this programme runs into a surprising limitation in that the dipole approximation breaks down in the *long* wavelength regime: as the wavelength increases, the electron has progressively longer times to accelerate in the field, and the magnetic Lorentz force $\mathbf{F}_m = \mathbf{v} \times \mathbf{B}$ becomes significant [7]. This pushes the electron along the laser propagation direction and, when strong enough, makes the electron wavepacket completely miss its parent ion, quenching all recollision phenomena, including in particular high harmonic generation [8–15].

Multiple schemes have been proposed to overcome this limitation, both on the side of the medium, from antisymmetric molecular orbitals [16] through relativistic beams of highly charged ions [17] to exotic matter like positronium [18] or muonic atoms [19] , and on the side of the driving fields, including counter-propagating mid-IR beams [20, 21], the use of auxiliary fields propagating in orthogonal directions [22], fine tailoring of the driving pulses [23], counter-propagating trains of attosecond pulses [24] in the presence of strong magnetic fields [25], and collinear and non-collinear x-ray initiated HHG [26, 27].

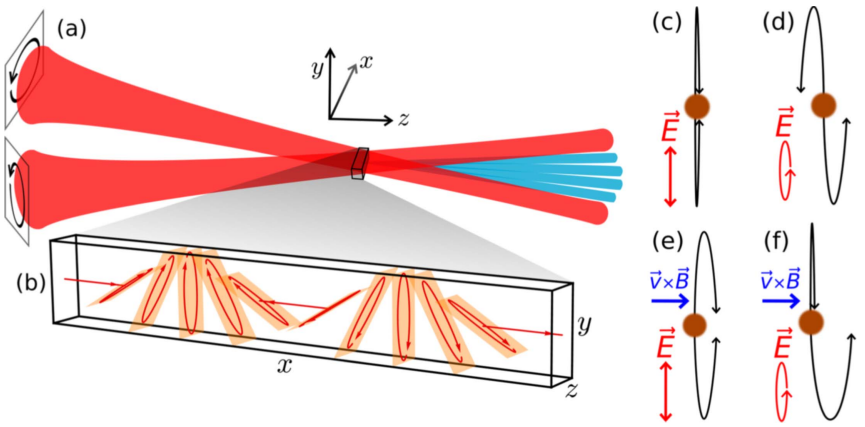

Figure 1. Two non-collinear circularly polarized beams (a) produce a polarization gradient across their focus in the transverse direction (b), including points with forwards ellipticity. This takes the usual linear trajectories (c) on a path to miss the ion (d), cancelling out the effect of the Lorentz force (e) to achieve one recollision per cycle (f), re-enabling the harmonic emission.

In general, however, the existing proposals are challenging in their implementation, facing limitations in the availability of laser sources, the decay lifetimes and bulk availability of unstable generation media, and complex phase-matching properties. Perhaps most promisingly, the magnetic force can also be compensated using a slight ellipticity in the propagation direction present in very tightly focused laser beams and in waveguide geometries [28, 29].

In this work we propose a simple method for attaining a forwards ellipticity that can act in the same direction as the Lorentz force, thereby re-enabling the harmonic emission in the presence of magnetic effects, through the use of two non-collinear counter-rotating circularly polarized beams of equal intensity and wavelength, as shown in figure 1(a). Normally, adding counter-rotating circular polarizations at the same frequency results in linear polarizations, but for non-collinear beams the planes of polarization do not quite match, and this means that at certain positions in the focus their components along the centerline will add constructively. This results in a forwards ellipticity: that is, elliptical polarizations with the unusual feature that the minor axis of the polarization ellipse is aligned along the centerline of the beam propagation.

This forwards ellipticity will tend to act in opposite directions for electrons released in each half-cycle (shown in figure 1(d)), as opposed to the Lorentz force, which acts always in the forwards direction (figure 1(e)), so one of the trajectories does return to the ion (figure 1(f)). One important consequence is that the symmetry between the two half-cycles is broken [29, 30], creating an unbalanced interferometer. This allows one to clearly show the action of the magnetic Lorentz force on the continuum electron in HHG with high sensitivity, to complement the experimental confirmation of the long-wavelength breakdown of the dipole approximation in ionization experiments [31, 32].

The interferometric quality of this scheme also has important consequences on the scaling with respect to the laser parameters. In general, the displacement of the wavepacket caused by the magnetic force scales as $d \propto F^2/2c\omega^3$, and the wavepacket width goes as $\Delta x \propto F^{1/2}/\omega(2I_p)^{1/4}$ [33], where F and ω are the driver amplitude and frequency, and I_p is the target's ionization potential[8], so the normalized displacement scales as

$$\zeta = \frac{d}{\Delta x} \propto \frac{(2I_p)^{1/4}}{2c}\frac{F^{3/2}}{\omega^2}. \tag{1}$$

If one attempts to detect this displacement via the wavepacket's electron density, as in the existing experiments [31, 32], or via observations of the drop-off in harmonic emission, the symmetric nature of the Gaussian wavepacket means that the relevant figure of merit is ζ^2, which is normally in the small-parameter limit. On the other hand, the unbalanced interferometer in our scheme produces even harmonics that scale linearly with ζ, and this in turn makes the observation of beyond-dipole effects accessible to a wide array of laser drivers, including sources that are already available, that would otherwise be unable to explore that regime.

Here, then, we extend the description of non-dipole HHG to cover non-collinear beam configurations. We show that non-collinear beams can indeed recover harmonic emission from damping by non-dipole effects, and that the even harmonics are readily accessible to currently available laser sources and can be used to observe signatures of the non-dipole effects in HHG.

The generation of harmonics using opposite circular polarizations, known as 'bicircular' fields, has been the subject of theoretical study for some time [34–39], and it reached fruition with the use of an ω–2ω collinear scheme to produce circularly polarized high harmonics [40, 41]. The use of non-collinear beams was demonstrated recently [42], and it permits the angular separation of the circular harmonics, with opposite

[8] We use atomic units unless otherwise stated.

helicities appearing on opposite sides of the far field, primed for generating circularly polarized attosecond pulses [39, 42].

Importantly, a non-collinear arrangement allows the use of a single frequency for both beams. As an initial approximation, the superposition of two opposite circular polarizations creates, locally, a linearly polarized field which permits the generation of harmonics. Here, the relative phase between the beams changes as one moves transversally across the focus, and this rotates the direction of the local polarization of the driving fields, and that of the emitted harmonics with it. This forms a 'polarization grating' for the harmonics, which translates into angularly separated circular polarizations in the far field [42].

Upon closer examination, however, the planes of polarization (i.e. the plane traced out by their circular polarization) of the two beams are at a slight angle, which means that they have nonzero field components along the centerline of the system. At certain points these components will cancel, giving a linear polarization, but in general they will yield the elliptical polarization shown in figure 1(b).

The possibility of forwards ellipticity in vacuum fields runs counter to our usual intuition, and so far it has only been considered in the context of a very tight laser focus [28, 29]. Our configuration provides a flexible, readily available experimental setup. In particular, it allows the focal spot size (and therefore the laser intensity) to be decoupled from the degree of forwards ellipticity. This ability is crucial, since it allows the ionization fraction to be tuned for phase-matching (although reaching perfect phase-matching conditions in the x-ray region requires very high pressure-length products because of the very long absorption lengths in the x-ray region).

To bring things on a more concrete footing, we consider the harmonics generated in a noble gas by two beams with opposite circular polarizations propagating in the x, z plane (as in figure 1(a)) with wavevectors

$$\mathbf{k}_\pm = k(\pm\sin(\theta),\ 0,\ \cos(\theta)), \tag{2}$$

where the angle θ to the centerline on the z axis, along $\mathbf{k} = \frac{1}{2}(\mathbf{k}_+ + \mathbf{k}_-)$, is typically small. The vector potential therefore reads

$$\begin{aligned}\mathbf{A}(\mathbf{r},\ t) &= \sum_\pm \frac{F}{2\omega}\begin{pmatrix}\cos(\theta)\cos(\mathbf{k}_\pm\cdot\mathbf{r}-\omega t)\\ \pm\sin(\mathbf{k}_\pm\cdot\mathbf{r}-\omega t)\\ \pm\sin(\theta)\cos(\mathbf{k}_\pm\cdot\mathbf{r}-\omega t)\end{pmatrix}\\ &= \frac{F}{\omega}\begin{pmatrix}\cos(\theta)\cos(kz\cos(\theta)-\omega t)\cos(kx\sin(\theta))\\ \cos(kz\cos(\theta)-\omega t)\sin(kx\sin(\theta))\\ \sin(\theta)\sin(kz\cos(\theta)-\omega t)\sin(kx\sin(\theta))\end{pmatrix},\end{aligned} \tag{3}$$

where $kx\sin(\theta)$ measures the relative optical phase between the beams (naturally measurable in radians or degrees) obtained transversely across the focus as a consequence of the nonzero angle between the beams' propagation directions.

As an initial approximation, for small θ, the polarization planes coincide, and the polarization becomes linear, with a direction which rotates across the focus:

$$\mathbf{A}(\mathbf{r},\ t) \approx \frac{F}{\omega}\begin{pmatrix}\cos(kx\sin(\theta))\\ \sin(kx\sin(\theta))\\ 0\end{pmatrix}\cos(\omega t), \tag{4}$$

where we set $z = 0$ and therefore just examine a single transverse plane. However, when taken in full, the vector potential has a slight ellipticity, with a maximal value of $\varepsilon = \sin(\theta)$ when $kx\sin(\theta) = \frac{\pi}{2}$, in which case

$$\mathbf{A}(\mathbf{r},\ t) = \frac{F}{\omega}\begin{pmatrix}0\\ \cos(\omega t)\\ -\sin(\theta)\sin(\omega t)\end{pmatrix}. \tag{5}$$

This forwards ellipticity acts in the same direction as the magnetic Lorentz force of the beam, so it can be used to control its effects as well as measure it, as exemplified in figure 1. As we shall show below, the field in (5) will produce even harmonics, through the symmetry breaking shown in figure 1. Since the ellipticity of the full field (3) varies across the focus, so does the strength of the even harmonics, and this spatial variation in their production is responsible for their appropriate far field behaviour.

In experiments, the beam half-angle θ will typically be small, on the order of 1°–5° [42], with corresponding ellipticities of up to $\varepsilon = \sin(\theta) \approx 9\%$, which is enough to counteract even significant magnetic drifts while still maintaining a flexible experimental scheme.

The generation of harmonics beyond the breakdown of the dipole approximation has been described in a fully relativistic treatment [13, 14], but this can be relaxed to the usual strong-field approximation [43] with appropriate modifications to include non-dipole effects [9–12, 22]. If a single beam is present, non-dipole terms break the dipole selection rules and produce even harmonics, but these are polarized along the propagation

direction and therefore do not propagate on axis. The use of multiple beams in the non-dipole regime allows for observable breakdowns of the selection rules [30], but the available results are only valid for restricted beam arrangements; here we extend the formalism of Kylstra *et al* [10–12, 22] to arbitrary beam configurations.

We start with the Coulomb-gauge Hamiltonian, with the spatial variation of $\mathbf{A}$ taken to first order in the electron's position $\mathbf{r}_e = \mathbf{r}_0 + \mathbf{r}$ about the nuclear position $\mathbf{r}_0$,

$$\begin{aligned}\hat{H}_V &= \frac{1}{2}(\hat{\mathbf{p}} + \mathbf{A}(\hat{\mathbf{r}}_e, t))^2 + \hat{V}_0 \\ &= \frac{1}{2}(\hat{\mathbf{p}} + \mathbf{A}(\mathbf{r}_0, t) + ((\hat{\mathbf{r}}_e - \mathbf{r}_0)\cdot\nabla)\mathbf{A}(\mathbf{r}_0, t))^2 + \hat{V}_0 \\ &= \frac{1}{2}(\hat{\mathbf{p}} + \mathbf{A}(\mathbf{r}_0, t) + (\hat{\mathbf{r}}\cdot\nabla)\mathbf{A}(\mathbf{r}_0, t))^2 + \hat{V}_0. \end{aligned} \tag{6}$$

We then perform a unitary transformation to $|\Psi_L\rangle = \mathrm{e}^{\mathrm{i}\hat{\mathbf{r}}\cdot\mathbf{A}(\mathbf{r}_0,t)}|\Psi_V\rangle$, as in the dipole case, and we define this as the length gauge. Here the Hamiltonian reads

$$\hat{H}_L = \frac{1}{2}(\hat{\mathbf{p}} + (\hat{\mathbf{r}}\cdot\nabla)\mathbf{A}(\mathbf{r}_0, t))^2 + \hat{\mathbf{r}}\cdot\mathbf{F}(t) + \hat{V}_0, \tag{7}$$

with $\mathbf{F}(t) = -\frac{\partial\mathbf{A}}{\partial t}(\mathbf{r}_0, t)$. Moreover, we neglect terms in $((\hat{\mathbf{r}}\cdot\nabla)\mathbf{A}(\mathbf{r}_0, t))^2$ for consistency, as they are of higher order in kr, to get our final Hamiltonian

$$H_L = \frac{\hat{\mathbf{p}}^2}{2} + \hat{\mathbf{r}}\cdot\mathbf{F}(t) + \hat{\mathbf{r}}\cdot\nabla\mathbf{A}(t)\cdot\hat{\mathbf{p}} + \hat{V}_0 = \hat{H}_{\mathrm{las}} + \hat{V}_0. \tag{8}$$

Here the gradient $\nabla\mathbf{A}(t)$ denotes a matrix whose i,jth entry is $\frac{\partial A_j}{\partial x_i}(\mathbf{r}_0, t)$, so in component notation the laser-only Hamiltonian reads

$$\hat{H}_{\mathrm{las}} = \frac{\hat{\mathbf{p}}^2}{2} + \hat{x}_j F_j(t) + \hat{x}_j\frac{\partial A_k}{\partial x_j}(t)\hat{p}_k, \tag{9}$$

with summations over repeated indices understood. (Here a change in the order of x_j and p_j changes the Hamiltonian in (9) by $i\nabla\cdot\mathbf{A}$, which vanishes for $\mathbf{A}$ in the radiation gauge, so the Hamiltonian is Hermitian [44].)

Within this model, the magnetic drift is caused embodied within the beyond-dipole coupling $\hat{\mathbf{r}}\cdot\nabla\mathbf{A}(t)\cdot\hat{\mathbf{p}}$, which is dominated by the derivative $\frac{\partial\mathbf{A}}{\partial z}$ along the centerline; this is then compensated by the longitudinal field component $F_z(t)$ produced by the forwards ellipticity.

Calculating the harmonic emission caused by the Hamiltonian (8) is essentially as simple as in the dipole case, which is by now standard material [2], and one only needs to modify the continuum wavefunction to include the non-dipole term. The required states here are non-dipole, non-relativistic Volkov states, which obey the Schrödinger equation for the laser-only Hamiltonian $\hat{H}_{\mathrm{las}}$ and which remain eigenstates of the momentum operator throughout. The dipole Volkov states are easily generalized by first phrasing them in the form

$$|\Psi_{\mathbf{p}}^{(V)}(t)\rangle = \mathrm{e}^{-\frac{\mathrm{i}}{2}\int^t \boldsymbol{\pi}(\mathbf{p},\tau)^2\mathrm{d}\tau}|\boldsymbol{\pi}(\mathbf{p}, t)\rangle, \tag{10}$$

where $|\boldsymbol{\pi}(\mathbf{p}, t)\rangle$ is a plane wave at the kinematic momentum $\boldsymbol{\pi}(\mathbf{p}, t) = \mathbf{p} + \mathbf{A}(t)$, and then finding appropriate modifications to $\boldsymbol{\pi}(\mathbf{p}, t)$.

To find these modifications, we first re-phrase the dynamics in terms of the pure plane wave component $|\boldsymbol{\pi}(\mathbf{p}, t)\rangle$, which obeys the Schrödinger equation

$$\mathrm{i}\frac{\mathrm{d}}{\mathrm{d}t}|\boldsymbol{\pi}(\mathbf{p}, t)\rangle = [\hat{\mathbf{r}}\cdot\mathbf{F}(t) + \hat{\mathbf{r}}\cdot\nabla\mathbf{A}(t)\cdot\hat{\mathbf{p}}]|\boldsymbol{\pi}(\mathbf{p}, t)\rangle, \tag{11}$$

which reduces to a simple equation of motion for the kinematic momentum $\boldsymbol{\pi}(\mathbf{p}, t)$:

$$\frac{\partial\boldsymbol{\pi}(\mathbf{p}, t)}{\partial t} - \frac{\mathrm{d}\mathbf{A}(t)}{\mathrm{d}t} = -\nabla\mathbf{A}(t)\cdot\boldsymbol{\pi}(\mathbf{p}, t), \tag{12}$$

which is then easily solved to first order in $1/c$ to the form

$$\boldsymbol{\pi}(\mathbf{p}, t, t') = \mathbf{p} + \mathbf{A}(t) - \int_{t'}^{t}\nabla\mathbf{A}(\tau)\cdot(\mathbf{p} + \mathbf{A}(\tau))\mathrm{d}\tau, \tag{13}$$

since $\int\nabla\mathbf{A}\mathrm{d}\tau \sim \frac{k}{\omega}A = \frac{1}{c}A$ for a monochromatic field.

Because of the presence of the integral in (13), we now require an additional reference time t' as an argument of $\boldsymbol{\pi}(\mathbf{p}, t, t')$, which was not required in the dipole case. If there is only a single beam, this is also not required: the integral is oscillatory, and the terms in t' can be dropped without further consequences [10–12, 22].

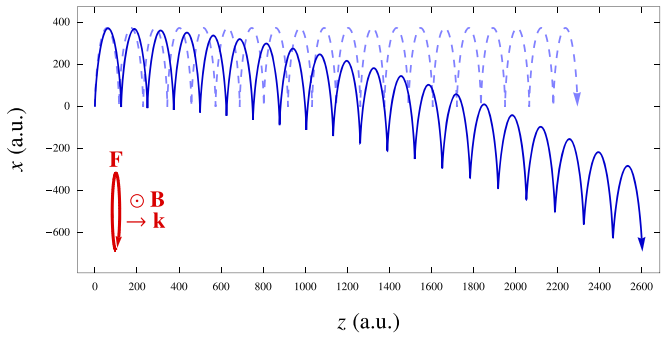

Figure 2. The classical trajectory (as integrated from Newton's equation of motion for the electric and magnetic fields at the nucleus; shown here projected on the x, z plane) of a particle released at rest at the peak of the field from (3) exhibits oscillations about a central position which accelerates uniformly transversely across the focus, with a parabolic trajectory. (The dashed trajectory ignores the effect of the magnetic force.) The effect is generally slight, and the parameters here (1.6 μm beams at 10^{15} W cm^{-2} with $\theta = 20°$, with the particle released at the nuclear position obeying $kx_0 \sin(\theta) = 15°$) are somewhat exaggerated, but the loss of periodicity in (14) if the t' dependence of $\boldsymbol{\pi}(\mathbf{p}, t, t')$ is ignored is serious. Similarly, the effect is only visually apparent over multiple oscillations, but even on the first oscillation the effect changes the time of recollision and therefore has a strong effect on the phase of the harmonic emission. This effect is also present for drivers with linear polarization in the common plane of propagation.

However, in the presence of multiple monochromatic beams, the integrand $\nabla\mathbf{A}(\tau) \cdot \mathbf{A}(\tau)$ can oscillate about a nonzero average, introducing a linearly-growing component to the integral $\int_{t'}^{t} \nabla\mathbf{A}(\tau) \cdot \mathbf{A}(\tau)\mathrm{d}\tau$. In this case, the reference time t' cannot be ignored, and for consistency it must be set at the ionization time for the HHG calculations [45].

This effect is real and physical, and it reflects the fact that the kinematic momentum $\boldsymbol{\pi}$ is subject to a linear walk-off: that is, a constant force in the x direction, orthogonal to the laser propagation direction, z, in addition to the usual oscillations (see figure 2). This constant force results from the interplay between the magnetic field and the z-direction velocity imparted by the elliptical electric field.

In practical terms the effect is small, but it affects the timing of the recollision event and therefore the phase of the emitted harmonics. As such, if not handled correctly it can introduce noise in a numerical spectrum at the same level as the signal.

Nevertheless, with the t' dependence factored in, the SFA solution can then be built on the non-dipole non-relativistic Volkov states in the standard fashion [2], by setting t' to the usual ionization time. This yields a harmonic dipole of the form

$$\mathbf{D}(t) = \int_{t_0}^{t} \mathrm{d}t' \int \mathrm{d}\mathbf{p}\, \mathbf{d}(\boldsymbol{\pi}(\mathbf{p}, t, t'))\mathrm{e}^{\mathrm{i}S(\mathbf{p},t,t')}\mathbf{F}(t') \cdot \mathbf{d}(\boldsymbol{\pi}(\mathbf{p}, t', t')) + \text{c.c.}, \tag{14}$$

where

$$S(\mathbf{p}, t, t') = I_p(t - t') + \frac{1}{2}\int_{t'}^{t} \boldsymbol{\pi}(\mathbf{p}, \tau, t')^2\mathrm{d}\tau, \tag{15}$$

is the (non-dipole) Volkov action, I_p is the ionization potential of the gas, and $\mathbf{d}(\mathbf{k}) = \langle\mathbf{k}|\hat{\mathbf{d}}|\Psi_g\rangle$ is the dipole transition matrix element from the ground state to a plane wave.

This harmonic dipole is sufficient to evaluate the harmonic emission from arbitrary beam configurations, and it can be further simplified by the use of the saddle-point approximation for the momentum integral, and the uniform approximation [46, 47] for the temporal integrations. Figures 3 and 4 show our calculations of the single-atom response at locations in the focus where the forwards ellipticity is maximal, using the field in (3) and setting the inter-beam angle θ to zero for the standard linear polarizations in figure 4. Our implementation is available from [48, 49].

At high intensities, shown in figure 4, the presence of non-dipole effects causes a drop-off in intensity [22]. Adding in a small amount of forwards ellipticity (at $\theta = 2°$) re-enables much of the harmonic emission, though further optimization is possible here. (At higher intensities, a fully relativistic treatment [13, 14] will become necessary, which will impact the extension of the plateau, but for a proof of concept of the harmonic recovery, the first-order treatment is sufficient.)

The breaking of the intra-cycle symmetry is visible at much lower intensities, as shown in figure 3 for fields at 800 nm and 1.6 μm. In particular, the non-dipole even harmonics begin to approach detectable intensities (between 0.1% and 1% of the intensity in the odd harmonics) even at 800 nm, and they are on par with the odd harmonics at 1.6 μm and 10^{15} W cm^{-2}. Such pulses can be produced using current optical parametric amplifiers, and they sit below the saturation intensity of helium, eliminating the need for highly charged species

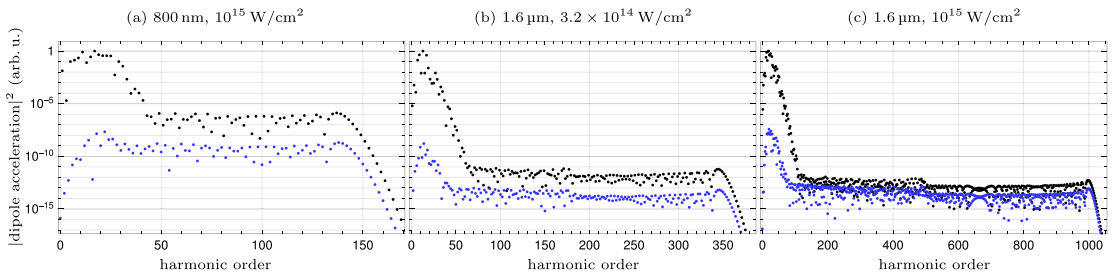

Figure 3. Harmonic spectra (● odd and ● even harmonics) produced in helium in the non-dipole regime for intensities of 3.2×10^{14} and 10^{15} W cm^{-2} and monochromatic fields of 800 nm and 1.6 μm at a beam half-angle of $\theta = 4°$, on arbitrary scales and eliminating z-polarized harmonics. The intensity ratio between even and odd harmonics varies from $\sim 10^{-3}$ for 800 nm drivers to $\sim$10% for strong mid-IR fields at 1.6 μm and 10^{15} W cm^{-2}, which are still accessible with current technology.

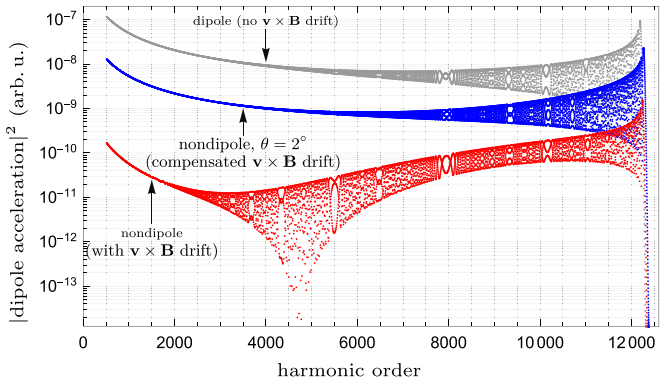

Figure 4. Above-threshold harmonic emission for a Ne^{6+} ion in an 800 nm field of intensity $I = 10^{17}$ W cm^{-2}, calculated in the uniform approximation using the first pair of quantum orbits, and discarding z-polarized harmonics. For linear polarization, the dipole approximation emission drops by two orders of magnitude when non-dipole effects are included, but adding in even a small forwards ellipticity, at $\theta = 2°$, can help recover the harmonic emission.

as a medium. The detection of non-dipole effects in HHG, then, can be done at rather moderate wavelengths and at intensities and with relatively simple experiments.

In addition to this, the even harmonics are also angularly separated from the dipole-allowed odd harmonics. This angular separation results from the conservation of momentum, and it has been clearly demonstrated for the dipole harmonics [42]: these must absorb an odd number of photons, but the conservation of spin angular momentum [37, 40] requires the harmonic to form from n photons of one beam and $n + 1$ photons from the other, resulting in a net transverse momentum of $\pm\hbar k_x = \pm\hbar k \sin(\theta)$ for the odd harmonics. The even harmonics represent the parametric conversion of an even number of photons, via the tensor operator $\hat{\mathbf{r}} \otimes \hat{\mathbf{p}}$: $\nabla \mathbf{A}$, and they can therefore absorb either zero transversal momentum (resulting in linear polarization along the y axis) or $\pm 2\hbar k_x$, with opposite circular polarizations. These even harmonics, then, appear at distinctly resolvable spots in the far field, which greatly simplifies their detection.

Similarly, it is important to remark that the harmonic emission will be produced under different forward-ellipticity conditions at different points transversely across the focus, and this will affect the intensity and phase of the emitted harmonics—and it will do so differently for different excursion times and therefore for different harmonic orders. Roughly speaking, the non-dipole displacement $d_{\mathrm{nd}} \sim F^2/2c\omega^3$ needs to be offset by the forwards ellipticity push $d_{F\varepsilon} \sim \gamma F\varepsilon/\omega^2$ (where $\varepsilon = \sin(\theta)\sin(kx\sin(\theta))$ and γ is a factor between ~ 1 and ~ 6 depending on the excursion time) to within the wavepacket width $\Delta x \sim F^{1/2}/\omega(2I_p)^{1/4}$; for equal $\zeta = d_{\mathrm{nd}}/\Delta x$, this selects wider regions of the focus if the non-dipole regime is reached via long wavelengths than if it is achieved at high intensities. In practice, however, there is a deep interplay between the harmonic recovery push (and its associated changes in the harmonic phase) and the macroscopic phase-matching conditions, which means that meaningful estimations of what fraction of the focal spot exhibit harmonic recovery require dedicated phase-matched propagation calculations dedicated to a specific configuration.

We see, then, that the introduction of forwards ellipticity into the harmonic generation permits both the recovery of the harmonic emission, even from strong cases of magnetic drift suppression, as well as the observation of clear signals of this mechanism in HHG experiments. This is done in an interferometric manner,

with a much more favourable linear scaling, and with the added benefit of a flexible and controllable scheme, bringing the experiment within reach of existing sources.

Acknowledgments

EP and MI acknowledge financial support from DFG and EPSRC/DSTL MURI grant EP/N018680/1. DDH, BRG, CGD, HCK and MMM thank AFOSR MURI grant FA9550-16-1-0121. EP thanks CONACyT and Imperial College London for support. BRG acknowledges support from the NNSA SSGF program.

ORCID iDs

Emilio Pisanty https://orcid.org/0000-0003-0598-8524

References

[1] Corkum P B and Krausz F 2007 Attosecond science *Nat. Phys.* **3** 381–7
[2] Ivanov M and Smirnova O 2014 Multielectron high harmonic generation: simple man on a complex plane *Attosecond and XUV Physics: Ultrafast Dynamics and Spectroscopy* ed T Schultz and M Vrakking (Weinheim: Wiley) pp 201–56
[3] Kohler M C *et al* 2012 Frontiers of atomic high-harmonic generation *Advances In Atomic, Molecular, and Optical Physics* (*Advances in Atomic, Molecular, and Optical Physics* vol 61) ed P Berman, E Arimondo and C Lin (New York: Academic) pp 159–208
[4] Popmintchev T *et al* 2012 Bright coherent ultrahigh harmonics in the keV x-ray regime from mid-infrared femtosecond lasers *Science* **336** 1287–91
[5] Hernández-García C *et al* 2013 Zeptosecond high harmonic kev x-ray waveforms driven by midinfrared laser pulses *Phys. Rev. Lett.* **111** 033002
[6] Zhu X and Wang Z 2016 Non-dipole effects on high-order harmonic generation towards the long wavelength region *Opt. Commun.* **365** 125–32
[7] Reiss H R 2000 Dipole-approximation magnetic fields in strong laser beams *Phys. Rev.* A **63** 013409
[8] Potvliege R M, Kylstra N J and Joachain C J 2000 Photon emission by He^+ in intense ultrashort laser pulses *J. Phys. B: At. Mol. Opt. Phys.* **33** L743
[9] Walser M W *et al* 2000 High harmonic generation beyond the electric dipole approximation *Phys. Rev. Lett.* **85** 5082–5
[10] Kylstra N J, Potvliege R M and Joachain C J 2001 Photon emission by ions interacting with short intense laser pulses: beyond the dipole approximation *J. Phys. B: At. Mol. Opt. Phys.* **34** L55–61
[11] Kylstra N J, Potvliege R M and Joachain C J 2002 Photon emission by ionis interacting with short laser pulses *Laser Phys.* **12** 409–14
[12] Chirilă C C 2004 Analysis of the strong field approximation for harmonic generation and multiphoton ionization in intense ultrashort laser pulses *PhD Thesis* Durham University (http://etheses.dur.ac.uk/10633/)
[13] Milošević D B and Becker W 2002 Relativistic high-order harmonic generation *J. Mod. Opt.* **50** 375–86
[14] Milošević D B, Hu S X and Becker W 2002 Relativistic ultrahigh-order harmonic generation *Laser Phys.* **12** 389–97
[15] Emelina A S, Emelin M Y and Ryabikin M Y 2014 On the possibility of the generation of high harmonics with photon energies greater than 10 keV upon interaction of intense mid-IR radiation with neutral gases *Quantum Electron.* **44** 470
[16] Fischer R, Lein M and Keitel C H 2006 Enhanced recollisions for antisymmetric molecular orbitals in intense laser fields *Phys. Rev. Lett.* **97** 143901
[17] Avetissian H K, Markossian A G and Mkrt-Chian G F 2011 High-order harmonic generation on atoms and ions with laser fields of relativistic intensities *Phys. Rev.* A **84** 013418
[18] Hatsagortsyan K Z, Müller C and Keitel C H 2006 Microscopic laser-driven high-energy colliders *Europhys. Lett.* **76** 29–35
[19] Müller C *et al* 2009 Exotic atoms in superintense laser fields *Eur. Phys. J. Spec. Top.* **175** 187–90
[20] Taranukhin V D 2000 Relativistic high-order harmonic generation *Laser Phys.* **10** 330–6
[21] Verschl M and Keitel C H 2007 Relativistic classical and quantum dynamics in intense crossed laser beams of various polarizations *Phys. Rev. ST Accel. Beams* **10** 024001
[22] Chirilă C C *et al* 2002 Nondipole effects in photon emission by laser-driven ions *Phys. Rev.* A **66** 063411
[23] Klaiber M, Hatsagortsyan K Z and Keitel C H 2007 Fully relativistic laser-induced ionization and recollision processes *Phys. Rev.* A **75** 063413
[24] Kohler M C *et al* 2011 Phase-matched coherent hard x-rays from relativistic high-order harmonic generation *Europhys. Lett.* **94** 14002
[25] Verschl M and Keitel C H 2007 Refocussed relativistic recollisions *Europhys. Lett.* **77** 64004
[26] Klaiber M *et al* 2008 Coherent hard x rays from attosecond pulse train-assisted harmonic generation *Opt. Lett.* **33** 411–3
[27] Kohler M C and Hatsagortsyan K Z 2012 Macroscopic aspects of relativistic x-ray-assisted high-order-harmonic generation *Phys. Rev.* A **85** 023819
[28] Lin Q, Li S and Becker W 2006 High-order harmonic generation in a tightly focused laser beam *Opt. Lett.* **31** 2163–5
[29] Galloway B R *et al* 2016 Lorentz drift compensation in high harmonic generation in the soft and hard x-ray regions of the spectrum *Opt. Express* **24** 21818–32
[30] Averbukh V, Alon O E and Moiseyev N 2002 Stability and instability of dipole selection rules for atomic high-order-harmonic-generation spectra in two-beam setups *Phys. Rev.* A **65** 063402
[31] Smeenk C T L *et al* 2011 Partitioning of the linear photon momentum in multiphoton ionization *Phys. Rev. Lett.* **106** 193002
[32] Ludwig A *et al* 2014 Breakdown of the dipole approximation in strong-field ionization *Phys. Rev. Lett.* **113** 243001
[33] Hatsagortsyan K Z *et al* 2008 Laser-driven relativistic recollisions *J. Opt. Soc. Am.* B **25** B92–103
[34] Eichmann H *et al* 1995 Polarization-dependent high-order two-color mixing *Phys. Rev.* A **51** R3414–7
[35] Long S, Becker W and McIver J K 1995 Model calculations of polarization-dependent two-color high-harmonic generation *Phys. Rev.* A **52** 2262–78

[36] Milošević D B, Becker W and Kopold R 2000 Generation of circularly polarized high-order harmonics by two-color coplanar field mixing *Phys. Rev.* A **61** 063403
[37] Pisanty E, Sukiasyan S and Ivanov M 2014 Spin conservation in high-order-harmonic generation using bicircular fields *Phys. Rev.* A **90** 043829
[38] Milošević D B 2015 Circularly polarized high harmonics generated by a bicircular field from inert atomic gases in the *p* state: a tool for exploring chirality-sensitive processes *Phys. Rev.* A **92** 043827
[39] Medišauskas L *et al* 2015 Generating isolated elliptically polarized attosecond pulses using bichromatic counterrotating circularly polarized laser fields *Phys. Rev. Lett.* **115** 153001
[40] Fleischer A *et al* 2014 Spin angular momentum and tunable polarization in high-harmonic generation *Nat. Photon.* **8** 543–9
[41] Kfir O *et al* 2015 Generation of bright phase-matched circularly-polarized extreme ultraviolet high harmonics *Nat. Photon.* **9** 99–105
[42] Hickstein D D *et al* 2015 Non-collinear generation of angularly isolated circularly polarized high harmonics *Nat. Photon.* **9** 743–50
[43] Lewenstein M *et al* 1994 Theory of high-harmonic generation by low-frequency laser fields *Phys. Rev.* A **49** 2117–32
[44] Cohen-Tannoudji C, Dupont-Roc J and Grynberg G 1989 *Photons and Atoms: Introduction to Quantum Electrodynamics* (New York: Wiley) p 197
[45] Pisanty E 2016 Electron dynamics in complex time and complex space *PhD Thesis* Imperial College London (http://doi.org/10044/1/43538)
[46] Figueira de Morisson Faria C, Schomerus H and Becker W 2002 High-order above-threshold ionization: the uniform approximation and the effect of the binding potential *Phys. Rev.* A **66** 043413
[47] Milošević D B and Becker W 2002 Role of long quantum orbits in high-order harmonic generation *Phys. Rev.* A **66** 063417
[48] Pisanty E 2016 RB-SFA: high harmonic generation in the strong field approximation via Mathematica https://github.com/episanty/RB-SFA, v2.1.1
[49] Pisanty E 2016 Figure-maker code and data for 'High harmonic interferometry of the Lorentz force in strong mid-infrared laser fields' *Zenodo* (http://doi.org/10.5281/zenodo.636667)